American Journal of Food Science and Technology, 2025, Vol. 13, No. 6, 156-163
Available online at http://pubs.sciepub.com/ajfst/13/6/2
Published by Science and Education Publishing
DOI:10.12691/ajfst-13-6-2

Modeling and Experimental Validation of Solar Drying of Maize in a Greenhouse-type Dryer under Tropical Climate

Kokou GNRONFOU[1,3], Tchamye Tcha-Esso BOROZE[1,2,3,*], Essohouna TAKOUGNADI[1,3]

[1]Department of Physics, University of Lomé, 01 B.P. 1515 Lomé, Togo
[2]Regional Center of Excellence for Electricity Management (CERME), University of Lomé, 01 B.P. 1515 Lomé, Togo
[3]Research Team on Agricultural Mechanization and Process Engineering (ERMAP), University of Lomé, 01 B.P. 1515 Lomé, Togo
*Corresponding author: tboroze@univ-lome.tg

Received November 20, 2025; Revised December 22, 2025; Accepted December 28, 2025

Abstract Solar drying is a sustainable post-harvest technique for maize valorization in tropical regions, but its performance strongly depends on thermal stability and solar radiation variability. This study presents the modeling and experimental validation of a solar greenhouse dryer, developed using coupled heat and mass balance equations expressed in matrix form. Simulations were compared with experimental data obtained from an instrumented prototype during three consecutive drying days. A strong agreement was found between simulated and measured values (MAE < 5°C; R^2 > 0.98). Internal air temperatures (45-57°C) ensured uniform evaporation, reaching a hygroscopic equilibrium moisture content of 10% within two days. The average thermal efficiency was 8.81%, indicating effective solar energy utilization. The obtained results confirm the relevance of solar-biomass coupling in stabilizing the drying process, improving energy efficiency, and maintaining the quality of dried maize under tropical climates.

Keywords: *solar drying, maize, greenhouse dryer, thermal performance, energy efficiency, tropical climate*

Cite This Article: Kokou GNRONFOU, Tchamye Tcha-Esso BOROZE, and Essohouna TAKOUGNADI, "Modeling and Experimental Validation of Solar Drying of Maize in a Greenhouse-type Dryer under Tropical Climate." *American Journal of Food Science and Technology*, vol. 13, no. 6 (2025): 156-163. doi: 10.12691/ajfst-13-6-2.

1. Introduction

Drying of agricultural products is a critical post-harvest process aimed at extending shelf life, reducing losses, and preserving nutritional and technological qualities [1,2]. In tropical regions, where high humidity and strong seasonal variability prevail, this operation plays a decisive role in food security. Among staple crops, maize (Zea mays L.) holds a strategic position in West Africa, serving as both a dietary staple and a key economic commodity. In Togo, maize covers more than 60% of cultivated land and represents the primary food crop. According to Agbenu and Koffi-Tessio [3], the maize sector has a strong wealth-creation potential but still suffers from post-harvest losses of 15-30%, mainly due to traditional open-air drying. These rudimentary methods depend heavily on weather conditions, leading to slow and uneven drying, fungal contamination, and degraded product quality [4,5].

Solar drying emerges as a sustainable, low-cost alternative adapted to African rural contexts [6,7,8]. It exploits an abundant, renewable, and non-polluting resource while reducing dependence on fossil fuels. However, direct-sun dryers are limited by dust contamination, high thermal losses, poor airflow uniformity, and sensitivity to solar fluctuations. The greenhouse-type solar dryer represents a major improvement, as it enhances solar radiation capture and retention, ensuring more stable and homogeneous internal temperatures [9,10]. Yet, the dryer's performance depends on multiple interacting parameters: air temperature, flow rate, relative humidity, and the thermophysical properties of the product.

A coupled heat and mass transfer model is therefore essential to understand the drying process and optimize thermal efficiency. While previous research has mainly focused on natural or forced convection systems [11,12,13], few studies have examined solar-biomass hybridization for maize drying in tropical environments. Such integration can ensure process continuity during cloudy periods while utilizing local biomass as a complementary energy source.

This study aims to model and simulate the thermal and moisture behavior of a greenhouse-type solar dryer equipped with a biomass-assisted heating system for maize drying. The model is based on discretized energy and mass balance equations solved in a matrix form, predicting the temporal evolution of air, product, cover, and floor temperatures, as well as the product moisture content. Simulated results were validated against experimental drying data collected in Lomé, Togo,

enabling the assessment of the model's accuracy and the dryer's energy performance.

This work contributes to the techno-energetic optimization of solar greenhouse drying systems adapted to tropical contexts. It proposes a hybrid, autonomous, and accessible system capable of minimizing post-harvest losses while ensuring product quality.

The paper is organized as follows: Section 2 describes the experimental setup and modeling assumptions; Section 3 details the mathematical formulation and numerical simulation; Section 4 presents and discusses the experimental and simulated results; and Section 5 concludes with overall performance evaluation and optimization perspectives for hybrid solar-biomass dryers.

2. Materials and Methods

2.1. Description of Drying Chambers

The drying greenhouse is a rectangular structure made of metal frames and covered with transparent plexiglass, featuring an arched roof to optimize solar capture. It rests on a concrete base for stability, with overall dimensions of 510 cm × 210 cm × 164 cm (L × W × H), and is oriented east-west to maximize sunlight exposure. The drying air enters through a mesh-covered opening at the base of the northwest side, flows through the products arranged on lateral shelves, and heats up by the greenhouse effect before absorbing moisture from the maize. The saturated air is then exhausted by a centrifugal fan (Sodeka CMP 620-2M, 0.37 kW) installed at the upper southeast face.

This solar dryer, designed by the Research Team on Agricultural Mechanization and Process Engineering (ERMAP) in collaboration with the Solar Energy Laboratory of the University of Lomé, was constructed and tested at the Agronomic Experimental Station of the School of Agronomy, University of Lomé (SEA-ESA/UL) (see Figure 1).

Figure 1. Greenhouse-type solar dryer

2.2. Mathematical Modeling

2.2.1. Simplifying Assumptions

The development of the mathematical model for the greenhouse-type solar dryer is based on the following simplifying assumptions:

(i). Absence of Air Stratification: The air inside the dryer is considered perfectly homogeneous, with uniform temperature and humidity distribution throughout the drying chamber.

(ii). Thin-Layer Drying Model: The drying process follows a thin-layer model, assuming that the agricultural products are spread in a uniform

(iii). thin layer to ensure consistent exposure to airflow and heat.

(iv). Constant Specific Heat: The specific heat capacities of air, the cover, and the product are assumed to remain constant during the entire drying process.

(v). Negligible Radiative Transfers: Radiative heat transfers between the ground and the cover, as well as between the ground and the product, are considered negligible [7,14,15,16,17].

2.2.2. Schematic Diagram of the Greenhouse Dryer

Figure 2 illustrates the main mechanisms of heat transfer within the greenhouse solar dryer from front, rear, and lateral perspectives. Three dominant transfer modes are identified:

- Conduction through the structural walls,
- Convection between the internal air and the surrounding surfaces, and
- Radiation between the product, the internal walls, and the sky.

The incident solar radiation I(t) represents the primary energy source, while the coefficients hc and hr denote the convective and radiative heat transfer coefficients, respectively. Air inlet (Ve) and outlet (Vs) openings control the airflow and humidity removal. The internal zones C1, C2, and C3 ensure a uniform thermal distribution throughout the chamber

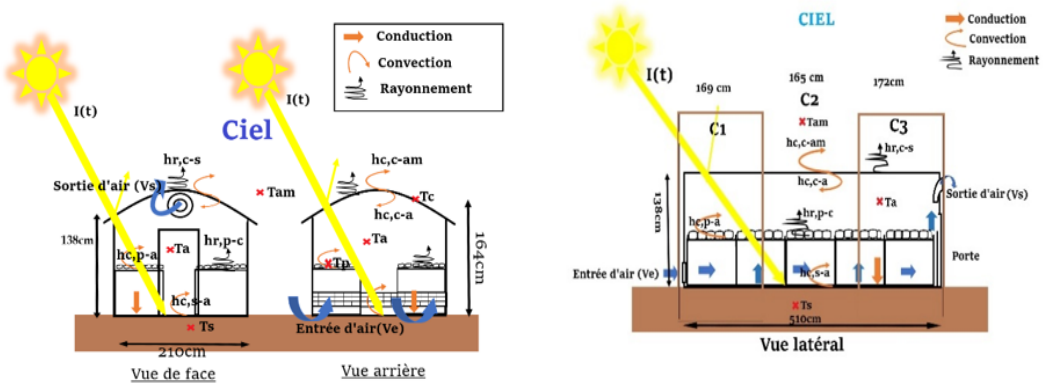

Figure 2. Schematic diagram of energy transfers within the greenhouse-type solar dryer

2.2.3. Energy and Mass Balance Equations

2.2.3.1. Energy Balance on the Cover

The total energy balance on the transparent cover of the greenhouse is expressed as follows:

$$m_c C_{pc}\frac{dT_c}{dt} = A_c h_{c,c-a}\left(T_a - T_c\right) + A_c h_{r,c-ciel}\left(T_{ciel} - T_c\right) + A_c h_{c,c-am}\left(T_{am} - T_c\right) + A_{pr} h_{r,pr-c}\left(T_{pr} - T_c\right) + A_C \alpha_c I_t \quad (1)$$

Such formulations are widely used in solar greenhouse dryer modeling [7,14,15,16,17], providing a robust foundation for analyzing transient energy flows and predicting the system's thermal response under varying climatic conditions.

2.2.3.2. Energy Balance of the Air Inside the Dryer

The thermal energy of the air inside the greenhouse-type solar dryer is determined by the sum of several heat transfer mechanisms:

$$\begin{aligned} m_a C_{pa}\frac{dT_a}{dt} &= A_{pr} h_{c,pr-a}\left(T_{pr} - T_a\right) + A_s h_{c,s-a}\left(T_s - T_a\right) + A_c h_{c,c-a}\left(T_c - T_a\right) \\ &- m_{pr} C_{pv}\left(T_{pr} - T_a\right)\frac{dM_{pr}}{dt} \\ &+ \left(\rho_a V_{out} C_{pa} T_{out?} - \rho_a V_{in} C_{pa} T_{in?}\right) \\ &+ U_c A_c\left(T_{am} - T_a\right) + \begin{bmatrix}\left(1-F_p\right)\left(1-\alpha_f\right) \\ +\left(1-\alpha_p\right)F_p\end{bmatrix} A_c \tau_c I_t \end{aligned} \quad (2)$$

2.2.3.3. Energy Balance of the Product

The thermal energy of the product is expressed as the sum of:

$$\begin{aligned} m_{pr} C_{ppr}\frac{dT_{pr}}{dt} &= A_{pr} h_{c,pr-a}\left(T_a - T_{pr}\right) + A_{pr} h_{r,pr-c}\left(T_c - T_{pr}\right) + A_{pr} h_{r,pr-s}\left(T_s - T_{pr}\right) \\ &+ m_{pr}\left[L_{pr} + C_{pv}\left(T_a - T_{pr}\right)\right]\frac{dM_{pr}}{dt} + A_{pr}\tau_c I_t F_p \alpha_p \end{aligned} \quad (3)$$

2.2.3.4. Energy Balance of the Concrete Floor

The thermal energy in the concrete floor results from:

$$\begin{aligned} m_s C_{ps}\frac{dT_s}{dt} &= A_s h_{c,s-a}\left(T_a - T_s\right) + A_s h_{D,s-g}\left(T_g - T_s\right) \\ &+ A_{pr} h_{r,pr-s}\left(T_{pr} - T_s\right) + \left(1 - F_{pr}\right) A_s \alpha_s I_t \end{aligned} \quad (4)$$

2.2.3.5. Mass Balance Equation

The humidity content of the air inside the dryer is governed by:

$$\begin{aligned} \rho_a V\frac{dH}{dt} &= m_{pr}\frac{dM_{pr}}{dt} \\ &- \rho_a V_{out} H_{out} A_{out} + \rho_a V_{in} H_{in} A_{in} \end{aligned} \quad (5)$$

2.2.3.6. Drying Kinetics of Maize

$$M_s = M_{se} + \left(M_{sc} - M_{se}\right).e^{-mt} \quad (6)$$

$$\frac{dM}{dt} = -m\left(M_s - M_{se}\right) \quad (7)$$

$$m = e^{\left(-\frac{571{,}38}{T_p} - 0{,}0055 h_r + 0{,}4609\right)} \quad (8)$$

where Ms is the moisture content at time t, Mse the equilibrium moisture, Msc the initial moisture, and mmm the drying constant dependent on product temperature Tpr and relative humidity hr [18].

2.2.3.7. Heat Transfer and Loss Coefficients

$$h_{r,c-ciel} = \epsilon_c \sigma\left(T_c^2 + T_{ciel}^2\right)\left(T_c + T_{ciel}\right) \quad (9)$$

$$h_{r,pr-c} = \epsilon_{pr} \sigma\left(T_c^2 + T_{pr}^2\right)\left(T_c + T_{pr}\right) \quad (10)$$

$$h_{r,pr-s} = \epsilon_{pr} \sigma\left(T_{pr}^2 + T_s^2\right)\left(T_{pr} + T_s\right) \quad (11)$$

$$T_{ciel} = 0{,}0552 T_{am}^{1,5} \quad (12)$$

$$h_{c,c-am} = 2{,}8 + 3{,}0 V_W \quad (13)$$

$$h_{D,s-g} = \frac{k_s}{\delta_s} \quad (14)$$

$$U_c = \frac{k_c}{\delta_c} \tag{15}$$

$$h_{c,s-a} = h_{c,c-a} = h_{c,pr-a} = \frac{N_u k_a}{D_h} \tag{16}$$

$$\mathrm{D_h} = \frac{4\mathrm{WD}}{2(\mathrm{W}+\mathrm{D})} \tag{17}$$

$$N_u = 0,0158 R_e^{0,8} \tag{18}$$

$$R_e = \frac{V_a D_h}{\upsilon} \tag{19}$$

These equations define convective and radiative heat transfer coefficients, accounting for ambient conditions, geometrical dimensions, and thermophysical properties. They are fundamental for solving the system's energy balance equations.

2.2.3.8. Matrix Formulation

The system of partial differential equations is discretized into a set of linear algebraic equations:

The discretization of the system's differential equations leads to a set of linear algebraic equations of the following form:

$$\begin{pmatrix} A_{11}A_{12}A_{13}A_{14} \\ A_{21}A_{22}A_{23}A_{24} \\ A_{31}A_{32}A_{33}A_{34} \\ A_{41}A_{42}A_{43}A_{44} \end{pmatrix} \times \begin{pmatrix} T_c^{t+\Delta t} \\ T_a^{t+\Delta t} \\ T_{pr}^{t+\Delta t} \\ T_s^{t+\Delta t} \end{pmatrix} = \begin{pmatrix} Y_1 \\ Y_2 \\ Y_3 \\ Y_4 \end{pmatrix} \tag{20}$$

This matrix formulation transforms the dynamic energy equations into a solvable linear system through matrix inversion, providing direct estimation of temperatures at each time step. This approach ensures numerical stability and rapid convergence, making it suitable for systems with slow thermal dynamics such as greenhouse-type solar dryers, where temperature gradients evolve gradually.

2.2.4. Energy Balance and Performance Evaluation

The mass flow rate of evaporated water ($\dot{m}_{eau}$) is defined as the amount of water removed per unit time, calculated based on the temporal variation in the product's moisture content weighted by its total mass:

$$\dot{m}_{eau} = -m_{pr} \cdot \frac{dX}{dt} \tag{21}$$

- η : The dryer efficiency expresses the evaporated water mass per unit area of the drying surface:

$$\eta = \left(\frac{\dot{m}_{eau}}{S} \right) \times 1000 \tag{22}$$

- $\dot{m}_a$: The required mass flow rate of air for water evaporation is derived from the energy balance:

$$\dot{\mathrm{m}}_{\mathrm{a}} = \frac{\dot{\mathrm{m}}_{\mathrm{eau}} \cdot \mathrm{L}_{\mathrm{pr}}}{\mathrm{C}_{\mathrm{pa}} \cdot (\mathrm{T}_{\mathrm{out}} - \mathrm{T}_{\mathrm{am}})} \tag{23}$$

- P_u : The useful power corresponds to the thermal power used to heat the drying air:

$$P_u = \dot{m}_a \cdot C_{pa} \cdot (T_a - T_{am}) \tag{24}$$

- P_s : The incident solar power received by the collector is given by:

$$P_s = I \times S \tag{25}$$

$$\xi = \left(\frac{P_u}{P_s} \right) \cdot 100 \tag{26}$$

- ξ : Finally, the collector efficiency (ξ) is defined as the ratio between the useful thermal power and the incident solar power [19].

These equations form the basis for the thermal performance analysis of the solar greenhouse dryer, enabling quantitative assessment of its energetic efficiency and adequacy under specific climatic and product conditions.

2.2.5. Experimental Protocol and Model Validation

The product temperatures were measured using three Type-K thermocouples, each with a precision of ±0.05 K, a response time below 20 s, and a measurement range suitable for solar-drying conditions. Air temperature and relative humidity inside the dryer were monitored using three Elitech RC-4/RC-4HC data loggers. These devices offer a measurement range of -30 to 60 °C (RC-4) and -40 to 85 °C (RC-4HC), with a temperature accuracy of ±0.5 °C within -20 to 40°C. The RC-4HC also measures relative humidity over 0–100% RH with an accuracy of ± 3% RH at 25 °C (for 20–80% RH). The air velocity in the greenhouse dryer was measured using a FVA935-TH5 thermo-anemometer, which provides a precision of ±0.20 m/s, allowing estimation of an average airflow rate of 0.102 m³/s through the dryer. Global solar irradiance was recorded with an RD-TSRS-04 pyranometer, featuring a measurement range of 0–2000 W/m², a resolution of 1 W/m², and a directional-response uncertainty below 30 W/m². Finally, the mass of the drying trays was monitored using a precision balance with an accuracy of ±2 g to compute the drying kinetics.

The experimental campaign was conducted from 9 to 11 August 2025 at the Agronomic Research Station of the University of Lomé to validate the numerical model of the greenhouse-type solar dryer applied to maize. Locally harvested maize cobs were shelled, and the grains were uniformly spread over ten trays (average mass 6.4 kg each) and arranged evenly inside the greenhouse (Figure 1). Three Type-K thermocouples (±0.05 K) recorded the product temperature at the inlet, middle, and outlet sections, connected to an Almemo 2390-8 data logger operating at a 15-minute acquisition interval. Simultaneously, three Elitech sensors measured the internal air temperature. The masses of trays m_1, m_2, and m_5 were recorded every hour using the precision scale to determine the drying curves. Solar irradiance was continuously monitored via the RD-TSRS-04 pyranometer.

Experimental measurements were compared with simulated results to assess model performance using the

following statistical indicators:

$$MAE = \frac{1}{n}\sum_{i=1}^{n}\left|T_{moy,i} - T_{air,i}\right| \quad (27)$$

$$RMSE = \sqrt{\left(\frac{1}{n}\sum_{i=1}^{n}\left(T_{moy,i} - T_{air,i}\right)^2\right)} \quad (28)$$

$$MAPE = \frac{1}{n}\sum_{i=1}^{n}\left|\frac{T_{moy,i} - T_{air,i}}{T_{moy,i}}\right| \times 100 \quad (29)$$

$$R^2 = 1 - \frac{\sum_{i=1}^{n}\left(T_{moy,i} - T_{air,i}\right)^2}{\sum_{i=1}^{n}\left(T_{moy,i} - \bar{T}_{moy}\right)^2} \quad (30)$$

These metrics estimate the precision, bias, and correlation between simulated and experimental temperatures, ensuring the model's reliability for coupled heat and mass transfer prediction.

2.2.6. Computational Process and Algorithm

A Python script was developed to solve the matrix system of energy equations representing the dryer's thermal behavior. The model simulates the transient evolution of the plexiglass cover, internal air, product, and concrete floor temperatures. The differential equations were discretized and solved numerically by matrix inversion, ensuring stable convergence and high numerical accuracy.

The code integrates multiple functions to calculate convective, radiative, and conductive heat transfer coefficients. Simulations performed over three consecutive days allow analysis of thermal dynamics, energy efficiency, and overall performance of the greenhouse solar dryer (Figure 3).

3. Results and Discussion

3.1. Energy Balance of the Solar Dryer

Figure 4 illustrates the hourly evolution of the simulated temperatures within the greenhouse-type solar dryer, including the air temperature (T air), product temperature (T product), cover temperature (T cover), floor temperature (T floor), and global solar irradiation (It). Measurements were taken during three consecutive drying days between 9:00 and 17:00. On the first day (09:57-16:42), the maximum solar irradiance reached 715.9 W/m², with an average air temperature of 53.6°C and a peak of 55.6°C. The product temperature averaged 46.4°C, peaking at 50.5°C. The second day (08:45-16:30) recorded a maximum irradiance of 1,123 W/m², an average air temperature of 55.2°C, and a product temperature averaging 51.9 °C with a peak of 57.8°C. On the third day (09:10-14:40), the maximum irradiance reached 1,009.6 W/m², while the air and product temperatures averaged 55.3°C and 51.4°C, respectively.

Figure 5 compares the simulated and experimental temperature profiles of air (T air) and product (T product) under the same irradiation conditions. The simulated air temperatures ranged between 53.6-55.3°C, while product temperatures varied from 46.4-51.9°C, with average standard deviations of 2.1°C and 5.6°C, respectively. The quantitative comparison reveals good agreement between simulation and experiment, with MAE = 2.62°C and RMSE = 3.16°C for product temperature, and MAE = 4.85°C and RMSE = 5.61°C for air temperature. The lowest error (RMSE = 2.1°C) occurred on Day 3, confirming optimal model-experiment consistency.

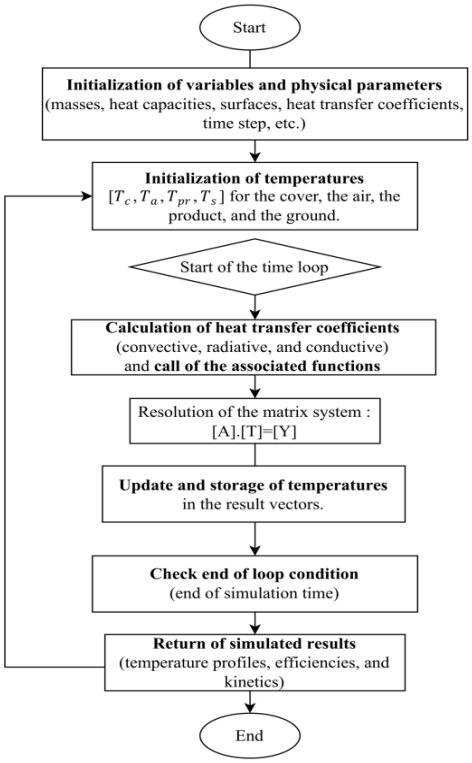

Figure 3. Flowchart of the linear system resolution

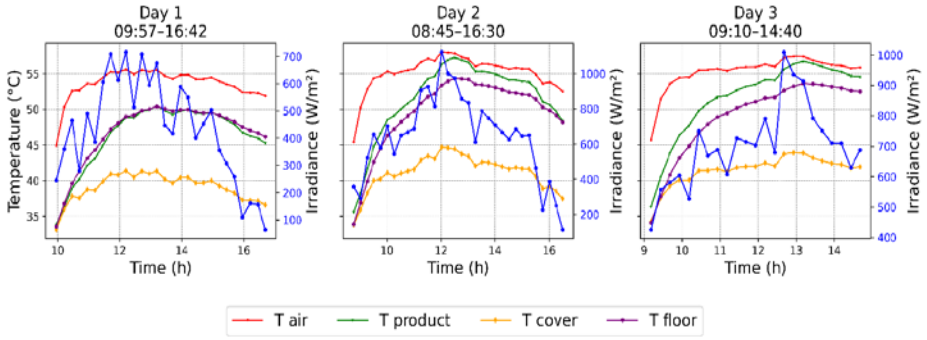

Figure 4. Hourly profile of simulated temperatures

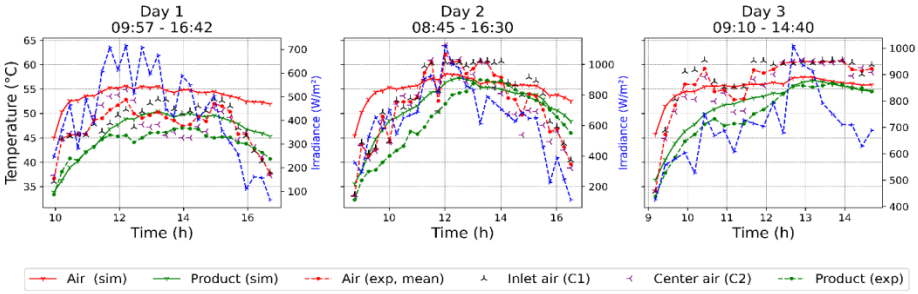

Figure 5. Comparison between simulated and experimental temperatures

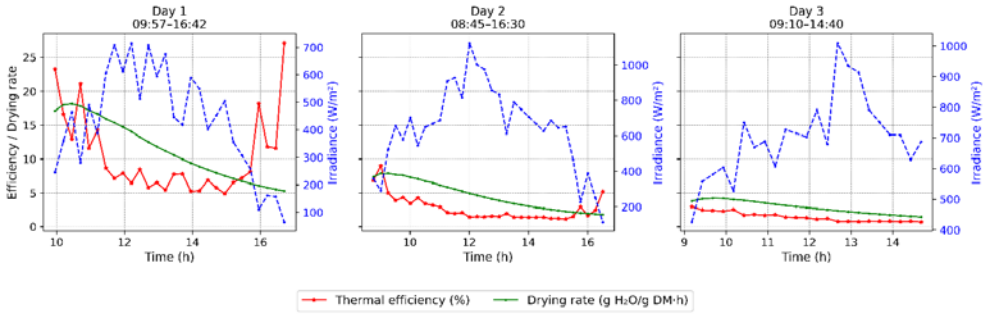

Figure 6. Energy performance profiles of the greenhouse solar dryer

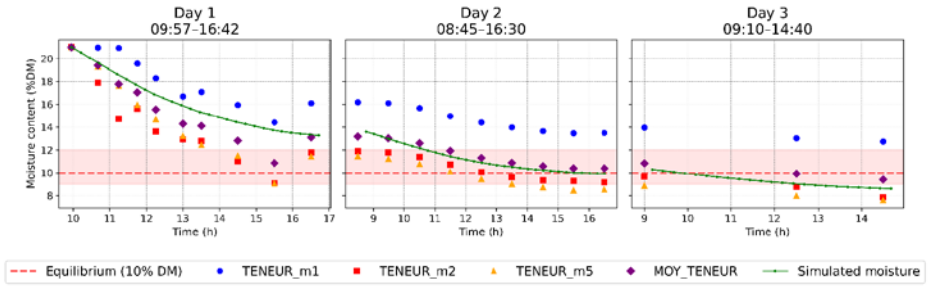

Figure 7. Evolution of the moisture content of maize

3.2. Solar Irradiance and Thermal Efficiency

Figure 6 presents the hourly evolution of thermal efficiency and maize drying rate during the three-day simulation. The average thermal efficiency reached 10.36 %, with an average drying rate of 11.40 g $H_2O \cdot kg^{-1}$ $DM \cdot h^{-1}$ on Day 1, reflecting intense drying activity. On Day 2, despite higher irradiance (mean = 646 W/m²; peak = 1,123 W/m²), the efficiency decreased to 1.62 % and the drying rate to 2.76 g $H_2O \cdot kg^{-1}$ $DM \cdot h^{-1}$, attributed to the reduced internal moisture gradient as drying progressed. Day 3, with average irradiance of 702.8 W/m², achieved 2.06 % efficiency and a drying rate of 4.12 g $H_2O \cdot kg^{-1}$ $DM \cdot h^{-1}$. The results indicate a gradual decline in drying rate over time, typical of hygroscopic materials, with an overall mean thermal efficiency of 8.81 %, peaking at 27.1 % on Day 1.

3.3. Drying Kinetics

Figure 7 shows the experimental and simulated moisture content evolution in maize during the three drying days. The mean moisture content (MOY_TENEUR) decreased from 21 % to about 10 % DM, representing a typical falling-rate drying period. The spatial gradient of

moisture, observed from m1 (inlet) to m5 (outlet), indicates faster drying near the outlet due to warmer and drier air. The simulation reproduced these dynamics accurately, with final values of 13.27 %, 9.93 %, and 8.60 % for Days 1, 2, and 3, respectively, achieving the hygroscopic equilibrium (10 % DM) from the second day onward. Statistical indicators confirm strong agreement (MAE = 0.76 %; RMSE = 1.02 %; R^2 = 0.90), validating the model's predictive capacity for drying kinetics.

3.4. Discussion

The three-day experimental and simulated results reveal a coherent thermal and mass behavior of the greenhouse-type solar dryer applied to maize. The air and product temperature profiles closely follow the trend of solar irradiance, with a slight delay attributable to the thermal inertia of the system. Maximum internal temperatures remained below 60°C, with average values of 54-55°C for air and 49-52°C for the product, which are optimal for gentle drying and the preservation of maize quality. The agreement between simulated and measured temperatures is satisfactory, with MAE and RMSE values remaining below 6°C, consistent with the deviations reported by Jain and Tiwari for similar greenhouse dryers [8]. The residual discrepancies arise mainly from the simplifying assumptions of the mathematical model-homogeneous air, thin-layer behavior, constant specific heat capacities, and negligible radiative exchanges as well as from the uncertainty of the sensors used: ±0.05 K for Type-K thermocouples, ±0.5°C for Elitech RC-4/RC-4HC sensors between –20 and 40°C, ±0.20 m/s for the FVA935-TH5 thermo-anemometer, and a directional response error below 30 W/m² for the RD-TSRS-04 pyranometer. Nevertheless, the consistency of the trends confirms the robustness of the coupled heat–mass transfer model.

The drying kinetics follow the classical pattern of agricultural products: an initial stage of fast moisture removal driven by external conditions, followed by a diffusion-controlled period where internal resistance dominates. The equilibrium moisture level (~10% dry basis) was reached by the second day, in agreement with Boroze et al. [6] for cereal drying under tropical conditions. During the second and third days, the drying rate decreased sharply (from ~11.4 to ~4.1 g $H_2O \cdot kg^{-1}$ $DM \cdot h^{-1}$), indicating that the limiting mechanism was no longer the available thermal energy but the internal diffusivity of the grains. In such situations, increasing the air temperature does not significantly accelerate the process, as previously observed by Akowuah and by Kumar for maize [17,20,21]. Internal temperatures around 45-57°C promote product safety while avoiding quality degradation, in accordance with findings showing that temperatures above 55°C can induce kernel cracking and reduce seed viability, whereas moderate temperatures (~50°C) preserve physicochemical integrity.

The overall thermal efficiency averaged 8.32%, with peak values reaching 27% under high irradiance. These results are comparable to those reported by Om Prakash, Anil Kumar, and Aumporn for forced-convection solar dryers [22,23]. Interestingly, the highest efficiencies were recorded between 15:00 and 16:00, when solar irradiance was decreasing while the internal temperature remained elevated due to the greenhouse effect, which acts as a thermal storage mechanism. This phenomenon has already been highlighted in previous studies and shows the ability of the dryer to retain heat even when the external energy supply diminishes. Conversely, the lower efficiency observed on days 2 and 3 is linked to the reduced moisture removal during the diffusion-controlled phase; because water evacuation is limited by internal resistance, increasing the temperature contributes minimally to useful heat conversion [24]. These observations also suggest that the dryer was under-loaded: with approximately 64 kg of maize, the thermal capacity of the system was not fully exploited. Increasing the loading density would improve both the efficiency and the overall usefulness of the captured solar energy, confirming that the structure can accommodate higher mass throughput without compromising performance.

From an operational perspective, the experimental period (August-November) corresponds to the maize harvest season in West Africa, which also overlaps with the rainy season characterized by unstable solar availability and high humidity, conditions that exacerbate postharvest losses. Even though the annual mean irradiance (~900 W/m²) is favorable for solar drying, the critical harvest window is particularly limiting. This context justifies the necessity of integrating a biomass auxiliary heating system to ensure continuous operation during cloudy periods, at night, or during rainfall events. Previous authors have shown that such hybrid configurations significantly reduce drying time and improve efficiency. Finally, internal temperatures near 52 °C naturally promote thermal disinfestation of maize. As demonstrated by Bosomtwe et al., maintaining 52 °C for three hours ensures complete insect deactivation without compromising grain quality [21,25]. Overall, these results validate the numerical model, confirm the effectiveness of the greenhouse dryer under tropical conditions, and highlight the relevance of a hybrid solar-biomass system to guarantee a faster, safer, and more reliable drying process throughout the year.

4. Conclusion and Perspectives

The present study confirms the thermal, energetic, and mass consistency of the hybrid greenhouse-type solar dryer applied to maize drying under tropical conditions. The numerical model, built on coupled heat and mass transfer balance equations, successfully reproduced the transient thermal regimes observed experimentally, with mean absolute deviations remaining below 5 °C. Internal temperatures ranging from 45 to 57 °C ensured uniform and effective drying while maintaining the technological and nutritional quality of maize. The attainment of the hygroscopic equilibrium (~10% dry basis) by the third day further validates the accuracy of the model and demonstrates the effectiveness of the solar–biomass hybrid configuration in reducing both drying time and energy demand.

The average thermal efficiency of 8.81% lies within the expected range for natural-convection solar dryers, indicating good solar energy capture and stable thermal redistribution within the structure. These performances,

combined with moderate and steady drying conditions, position the proposed system as a sustainable and economically viable alternative to fossil-fuel-based dryers in tropical agricultural environments.

Building on these findings, two major improvements are envisioned. First, a biomass auxiliary heating system will be integrated through a finned-tube heat exchanger directly coupled to a biomass combustion chamber. In this configuration, ambient air will be preheated inside the exchanger before entering the greenhouse and subsequently extracted by a centrifugal fan positioned at the outlet, ensuring optimal airflow circulation and thermal homogeneity. The auxiliary system will be equipped with a PID-based automatic temperature regulation unit, designed to maintain the drying air within the optimal range of 50–55 °C during cloudy periods, sudden irradiance drops, or night-time operation. Second, the system's performance will be further enhanced through aerodynamic optimization of the airflow pathway, including adjustments to air velocity, tray spacing, and internal geometry to improve thermal uniformity and ensure consistent drying rates.

Overall, these developments aim to increase energy efficiency, stabilize the process under fluctuating environmental conditions, and improve final product quality. The integration of an intelligent, adaptive biomass-assisted heating module will extend the operational flexibility of the dryer and make it better suited to the climatic and practical constraints of tropical agricultural systems, particularly during the rainy harvest season when solar availability is highly variable. This work thus lays the foundation for the next generation of hybrid solar dryers combining sustainability, efficiency, and year-round reliability.

Conflict of Interest Statement

This research did not receive any specific funding from public, commercial, or non-profit organizations.

Declaration of generative AI and AI-assisted technologies in the manuscript preparation process.

During the preparation of this work, the author used OpenAI's ChatGPT to assist in linguistic refinement and content structuring to ensure clearer and more concise expression in English. After using this tool, the author reviewed and modified the content as necessary and assumes full responsibility for the final publication.

References

[1] Bonazzi C, Bimbenet J-J. Séchage des produits alimentaires - Principes. Agroalimentaire 2003.

[2] Charreau A, Cavaillé R. Séchage. Théorie et calculs. Opérations Unit Génie Réaction Chim 1995.

[3] Agbenu NK. COMPETITIVITE DE LA PRODUCTION DU MAÏS AU TOGO: une étude comparative des zones agro-écologiques. J Rech Sci Univ Lomé 2016.

[4] Baoua IB, Amadou L, Bakoye ON, Abdoulaye O, Baributsa D, Murdock LL. Maize quality in markets in four West African countries. J Stored Prod Res 2016; 69: 26–30.

[5] Boroze TTE. Outil d'aide à la conception de séchoirs pour les produits agricoles tropicaux. thesis. Université de Lomé, 2011.

[6] Boroze TT-E, Azouma YO, Ahanogbe K, Barate M. Séchage solaire de céréales: cinétiques, évaluations thermo-hygrométrique et énergétique 2018.

[7] Intawee P, Janjai S. Performance evaluation of a large-scale polyethylene covered greenhouse solar dryer. Int Energy J 2011; 12: 39–52.

[8] Jain D, Tiwari GN. Effect of greenhouse on crop drying under natural and forced convection II. Thermal modeling and experimental validation. Energy Convers Manag 2004; 45: 2777–93.

[9] ELkhadraoui A, Kooli S, Farhat A. Etude expérimentale de la performance d'un séchoir solaire de type serre: séchage de piment. 5ème Sémin Maghréb Sur Sci Technol Séchage 2015.

[10] Tuncer AD, Sözen A, Khanlari A, Amini A, Şirin C. Thermal performance analysis of a quadruple-pass solar air collector assisted pilot-scale greenhouse dryer. Sol Energy 2020;203:304–16.

[11] Chi X, Tang S, Song X, Rahimi S, Ren Z, Han G, et al. Energy and quality analysis of forced convection air-energy assisted solar timber drying. Energy 2023; 283: 128718.

[12] Choudhary AK, Hazarika MK. Modélisation et analyse thermique d'un séchoir solaire intégré pour le gingembre (*Zingiber officinale*) et la qualité du produit. J Stored Prod Res 2024; 106: 102313.

[13] Sallam YI, Aly MH, Nassar AF, Mohamed EA. Solar drying of whole mint plant under natural and forced convection. J Adv Res 2015; 6: 171–8.

[14] Colorado A, Morales O, Ossa D, Amell A, Chica E. Modeling the optimal condition for drying rumen contents using a solar greenhouse dryer. Case Stud Therm Eng 2022; 30.

[15] Janjai S, Lamlert N, Intawee P, Mahayothee B, Bala BK, Nagle M. Experimental and simulated performance of a PV-ventilated solar greenhouse dryer for drying of peeled longan and banana. Sol Energy 2009; 83: 1550–65.

[16] Janjai S, Intawee P, Kaewkiew J, Sritus C, Khamvongsa V. A large-scale solar greenhouse dryer using polycarbonate cover: Modeling and testing in a tropical environment of Lao People's Democratic Republic. Renew Energy 2011; 36: 1053–62.

[17] Kumar L, Hasanuzzaman M, Rahim NA, Islam MM. Modeling, simulation and outdoor experimental performance analysis of a solar-assisted process heating system for industrial process heat. Renew Energy 2021; 164: 656–73.

[18] Andriazafimahazo L, Rakotomahevitra A, Ramamonjisoa B, Zeghmati B. Modélisation de la vitesse de séchage du maïs. Afr Sci Rev Int Sci Technol 2010; 5.

[19] Deng S, Yu Y, Yao L, Liu H, Xu J, Huo H, et al. Energy efficiency analysis of a rotating-drum dryer using hot steel balls for converter sludge. Case Stud Therm Eng 2023; 49: 103389.

[20] Akowuah JO, Maier D, Opit G, McNeill S, Amstrong P, Campabadal C, et al. Drying Temperature Effect on Kernel Damage and Viability of Maize Dried in a Solar Biomass Hybrid Dryer. Open J Appl Sci 2018; 8: 506–17.

[21] Zhang Z, Xu C, Zhang S. VACUUM DRYING CHARACTERISTICS OF MAIZE: KINETICS, CRACKING AND GERMINATION QUALITY. 2007.

[22] Aumporn O. Contribution à l'étude des performances d'un séchoir serre avec stockage de chaleur dans des matériaux à changement de phase. UNIVERSITE DE PERPIGNAN, 2017.

[23] Kumar A, Tiwari GN. Effect of shape and size on convective mass transfer coefficient during greenhouse drying (GHD) of Jaggery. J Food Eng 2006; 73: 121–34.

[24] Takougnadi E, Boroze T-ET, Azouma YO. Étude des conditions optimales de séchage de l'oignon : efficacité énergétique, qualités nutritionnelle et organoleptique. 19ème Journ Sci Annu SOACHIM 2018.

[25] Bosomtwe A, Danso JK, Osekre EA, Opit GP, Mbata G, Armstrong P, et al. Effectiveness of the solar biomass hybrid dryer for drying and disinfestation of maize. J Stored Prod Res 2019; 83: 66–72.